# LIQUIDUS TEMPERATURE AND ALUMINA SOLUBILITY IN THE SYSTEM $Na_3AlF_6$-$AlF_3$-LiF-$CaF_2$-$MgF_2$

A. Solheim, S. Rolseth, E. Skybakmoen, and L. Støen
SINTEF Materials Technology, N-7034 Trondheim, Norway

Å. Sterten and T. Støre
The Norwegian Institute of Technology, N-7034 Trondheim, Norway

## Abstract

The liquidus temperature for primary crystallization of cryolite in the system $Na_3AlF_6$-$AlF_3$-LiF-$CaF_2$-$MgF_2$ was determined by thermal analysis. The data were fitted to an empirical equation, valid from 1011 °C to approximately 800 °C. The alumina solubility was determined from the weight loss of a rotating sintercorundum disc. The investigated temperature range was 850-1050 °C, and the data were fitted to an empirical expression. The data are also presented in the form of quasi-binary phase diagrams.

## Introduction

The main component of the electrolyte (bath) in commercial aluminium electrolysis cells is cryolite, which has a melting point of 1011 ± 1 °C[1,2]. In addition to cryolite, conventional electrolytes contain 5-13 wt% $AlF_3$, 3-7 wt% $CaF_2$, and 1-5 wt% $Al_2O_3$. Some companies have also introduced other additives such as LiF and $MgF_2$. An industrial cell with conventional electrolyte usually operates in the temperature range 950 - 980 °C, depending on bath composition, which is about 5-15 °C above the corresponding liquidus temperature for primary cryolite crystallization. Addition of LiF to this melt increases the electrical conductivity[3,4] and lowers the liquidus temperature. However, the main purpose of using additives such as LiF and $MgF_2$ is the potential of increasing the current efficiency with respect to aluminium[5,6].

Sodium cryolite ($Na_3AlF_6$) is the main bath constituent due to its high alumina solubility. Previously, alumina was added batchwise to the electrolyte, and a high solubility was regarded as a prerequisite in order to minimize the accumulation of alumina sludge underneath the metal pad. In the last decades, more sophisticated methods with nearly continuous feeding of alumina has been developed, and the restrictions concerning solubility have been somewhat lifted. In this situation some interest in alternative electrolyte compositions, *i.e.*, low melting baths, has emerged. By the introduction of low melting baths one may achieve higher current efficiency, lower carbon consumption, and, possibly, prolonged cell life and easier adaption of inert electrode materials[7,8]. However, the rate of solution of alumina and the solubility limit are still critical factors. Reliable data for the liquidus temperature and alumina solubility are therefore key parameters in the operation of commercial aluminium electrolysis cells and for the development of low melting electrolytes.

Several research groups have developed model equations describing liquidus surfaces for compositions roughly corresponding to the conventional electrolytes[9-13]. Therefore, it should be emphasized that most of the equations are valid for a limited range of compositions. Phase equilibria in cryolite based melts have been studied by thermal analysis (TA), by differential thermal analysis (DTA), by visual observations, and by quenching techniques[9-15]. In the region of primary cryolite crystallization, TA has proven to give accurate freezing point depression data[1,2,13,14].

The alumina solubility is also relatively well established in the normal range of electrolyte compositions[10,15,16,19]. Alumina liquidus equations were derived by Dewing[9] and by Skybakmoen *et al.*[19]. The data are more scarce at high contents of additives and lower temperatures, although a number of $Na_3AlF_6$-$AlF_3$-$Al_2O_3$-$M_aX_b$ ternary and quarternary liquidus diagrams have been partly investigated[17]. In most cases, the alumina liquidus was established by visual methods[15] or by quenching techniques[10,16]. However, the nucleation of alumina crystals is very sluggish[15,18], and due to the steep alumina liquidus surface a considerable supercooling and oversaturation will easily occur. The solubility limit as found by these methods would therefore tend to be too high, which is reflected in some of the work with alumina-saturated cryolitic melts[17].

The purpose of the present work was to establish 1) the liquidus temperature for primary cryolite crystallization and 2) the alumina solubility for a wide range of temperatures and compositions in the system $Na_3AlF_6$-$AlF_3$-$CaF_2$-$MgF_2$-LiF, and, furthermore, to derive practical equations describing 1) the liquidus temperature and 2) the alumina solubility as functions of temperature and composition based on the experimental data. The equations presented here do not deviate much from our earlier work[13,19] which in fact was based on much of the same experimental data. The composition range has been somewhat extended, however.



G. Bearne et al. (Eds.), *Essential Readings in Light Metals*

## Experimental

### Chemicals

Hand-picked natural Greenland cryolite with a melting point of 1011 ± 1 °C was used. $AlF_3$ was purified in our own laboratory by sublimation, while $CaF_2$, $MgF_2$, LiF, KF and calcined alumina were high quality chemicals containing very small amounts of impurities.

### Liquidus Temperature

The liquidus temperature for primary cryolite crystallization was determined by thermal analysis, performed in a vertical alumina tube furnace under argon atmospere. The experimental arrangement is shown in Figure 1 a). The crucible was usually made of nickel (61 mm inner dia.), while the lid and the thermocouple protection tube were made of high quality graphite. Supercooling of the melt was prevented or reduced by using a slow cooling rate (0.5 or 0.7 °C/min) and vigorous stirring. The stirrer was made of either nickel or high quality graphite. In some cases, frequent seeding of small cryolite crystals to the melt was applied through a separate sintercorundum tube (not shown in the figure). Further details on the experimental set-up and procedures can be found elsewhere[2,20].

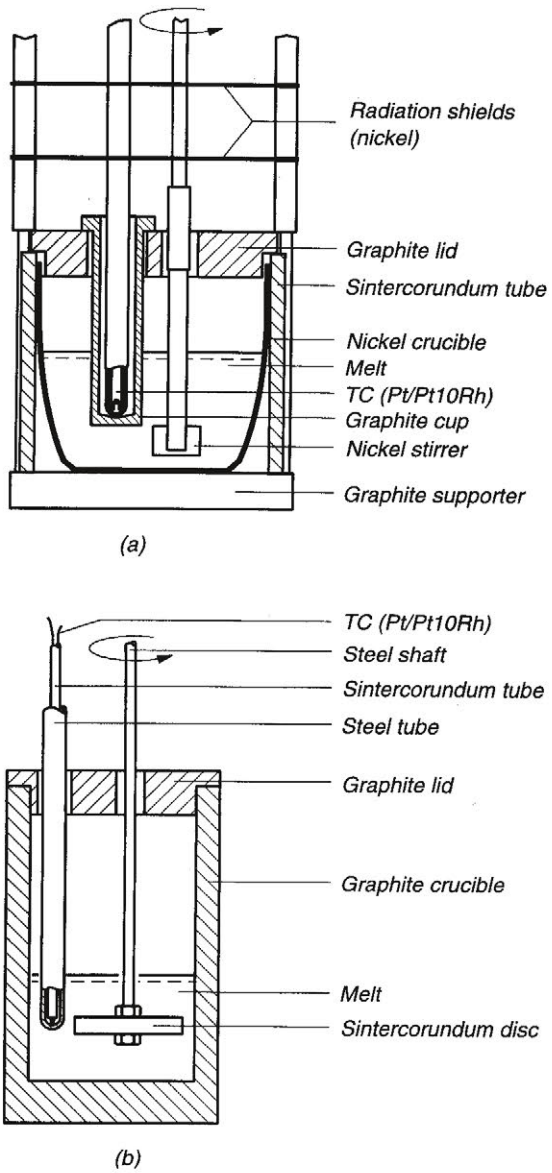


**Figure 1.** Experimental arrangements for determination of the liquidus temperature (a) and the alumina solubility (b).

### Alumina Solubility

The alumina solubility was determined by measuring the weight loss of a rotating sintercorundum disc. The disc was 40 mm in diameter and 6 mm thick, and it contained minimum 99.7 % $Al_2O_3$. The disc was submerged into the melt and fastened to a rotating stainless steel shaft, as shown in Figure 1 b). Approximately 200 g of melt was kept in a graphite crucible provided with a graphite lid. The temperature was recorded by a calibrated Pt-Pt10Rh thermocouple located inside a stainless steel protection tube.

The experiment started by lowering the disc assembly into the melt. The contact time between the disc and the melt was 6 (occasionally 4) hours and the disc was usually rotated at 340 rpm. At the end of the experiment the disc was lifted above the melt which was allowed to cool down to room temperature. The frozen melt which adhered to the disc was removed mechanically, and weighed together with the melt from the crucible. The disc was further cleaned by dissolving the remaining salt in a hot aquous solution of $AlCl_3$. The alumina saturation concentration was then calculated from the weight change of the disc, referred to the total amount of melt at the end of the experiment.

Blind tests performed in alumina-saturated melts showed a slight increase in the weight of the disc, equivalent to 0.05 - 0.15 wt % of the total bath weight, probably depending on the porosity of sintered disc. Consequently, all the calculated alumina solubilities were adjusted upwards by 0.1 wt%. Duplicated runs agreed to ±0.2 wt% $Al_2O_3$, which is well within our estimated total uncertainty of ±0.3 wt%. Further discussion concerning the method can be found elsewhere[19,21].

## Results and Discussion

### Liquidus Temperature for Primary Cryolite Crystallization

For the equilibrium reaction,

$$Na_3AlF_6\,(l) = Na_3AlF_6\,(s) \qquad (1)$$

the $Na_3AlF_6$ crystallization surface can be described by the relation,

$$RT \ln\left(\frac{a(l)}{a(s)}\right) = -\Delta H_f\left(1 - \frac{T}{T_f}\right) \qquad (2)$$

where a($l$) and a($s$) represent activities of $Na_3AlF_6$ in the liquid and the solid state, respectively, and $\Delta H_f$ is the heat of fusion of pure $Na_3AlF_6$ (106745 J/mol[22]) at the melting point $T_f$ = 1284 K (1011 °C). If there is no solid solubility in the system then, by definition, a($s$) = 1. With small additions of solute $B$, Raoult's law is valid for the solvent $A$ (cryolite) and the following equation can be derived in the absence of solid solubility,

$$\frac{dt}{d[B]} = -\frac{RT_f^2}{\Delta H_f} \cdot \frac{n M_A}{100 M_B} \qquad [°C/wt\%] \qquad (3)$$

where t is the liquidus temperature, the square brackets denote concentration of solute in wt%, n is the number of new species being formed per molecule of $B$, and M is the molar weight. It is easily predicted that a mathematical description of all the binary cryolite liquidus curves will be a good starting position for deriving an equation for the primary crystallization of $Na_3AlF_6$ in the multicomponent system.

Based on the experimental points shown in Figures 2-7 and in Table I, the following empirical equation was derived,

$$\begin{aligned} t = {} & 1011 + 0.50[AlF_3] - 0.13[AlF_3]^{2.2} \\ & - \frac{3.45[CaF_2]}{1 + 0.0173[CaF_2]} \\ & + 0.124[CaF_2][AlF_3] - 0.00542\left([CaF_2][AlF_3]\right)^{1.5} \\ & - \frac{7.93[Al_2O_3]}{1 + 0.0936[Al_2O_3] - 0.0017[Al_2O_3]^2 - 0.0023[AlF_3][Al_2O_3]} \\ & - \frac{8.90[LiF]}{1 + 0.0047[LiF] + 0.0010[AlF_3]^2} \\ & - 3.95[MgF_2] - 3.95[KF] \end{aligned} \qquad (4)$$

where t is the temperature in °C and the square brackets denote wt% of components in the system $Na_3AlF_6$-$AlF_3$-$CaF_2$-$Al_2O_3$-LiF-$MgF_2$-KF. The composition limitations are proposed to be: $[AlF_3] \approx [CaF_2] \approx [LiF] < 20$ wt%, $[MgF_2] \approx [KF] < 5$ wt%, and $[Al_2O_3]$ up to the saturation concentration for primary crystallization of $Al_2O_3$. The standard deviation is 1.45 °C when all the 184 experimental points are included.

$Na_3AlF_6$-$AlF_3$. Figure 2 shows the cryolite liquidus curve in the system $Na_3AlF_6$-$AlF_3$. The results clearly indicate that the primary freezing temperature increases slightly by small additions of $AlF_3$.

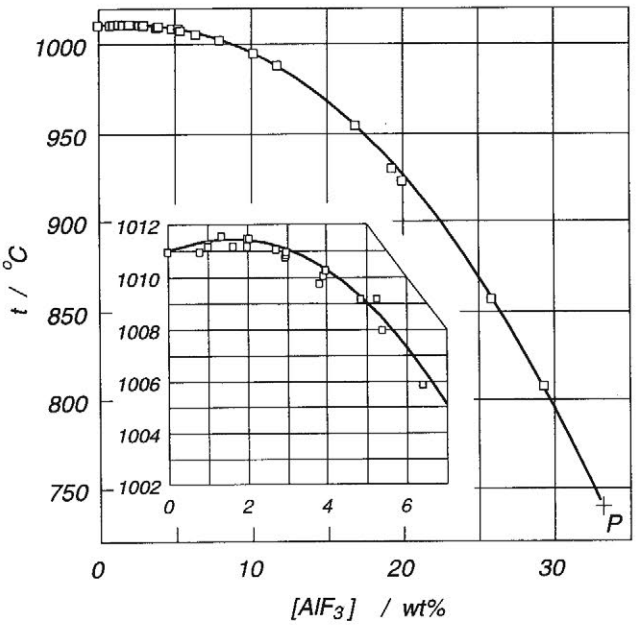


**Figure 2.** The liquidus temperature for the system $Na_3AlF_6$-$AlF_3$. The curve represents Eq. (4). P is the peritectic point.

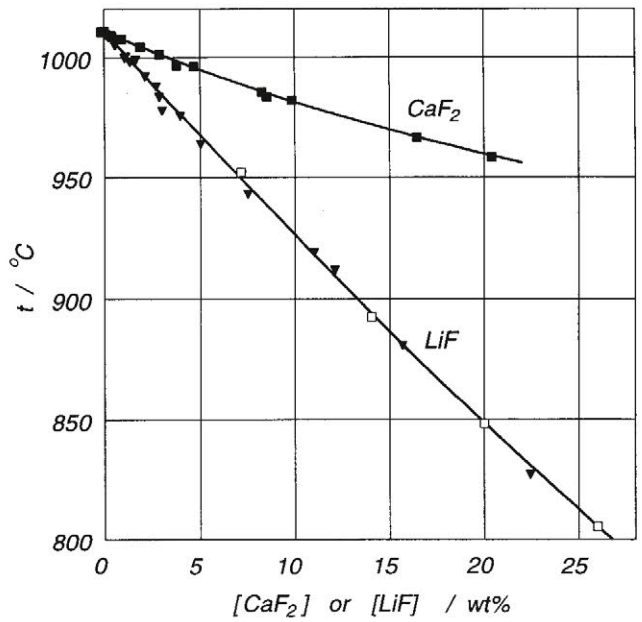


**Figure 3.** Liquidus curves for the systems $Na_3AlF_6$-$CaF_2$ and $Na_3AlF_6$-LiF. Filled squares - Holm[23], filled triangles - Holm[24], open squares - this work. The curves represent Eq. (4).

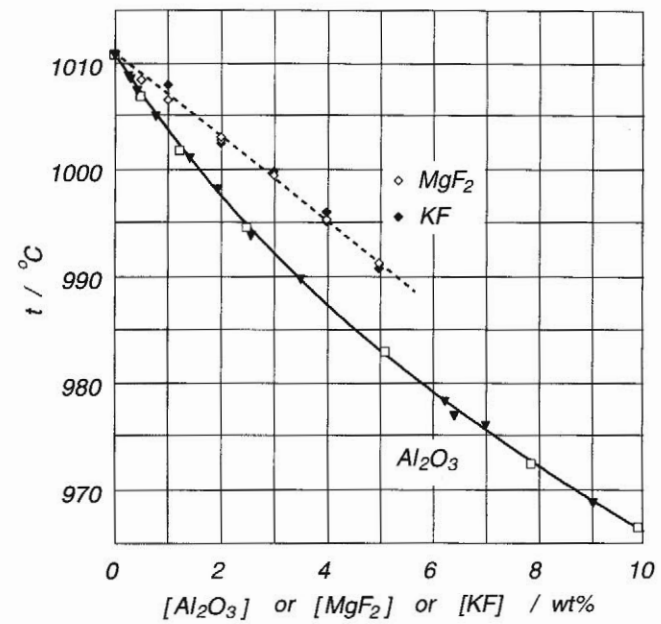


**Figure 4**. The cryolite liquidus curves for the systems $Na_3AlF_6$-$Al_2O_3$, $Na_3AlF_6$-$MgF_2$, and $Na_3AlF_6$-KF. Filled triangles - Holm (see ref. 22), other symbols - this work, lines - Eq. (4).

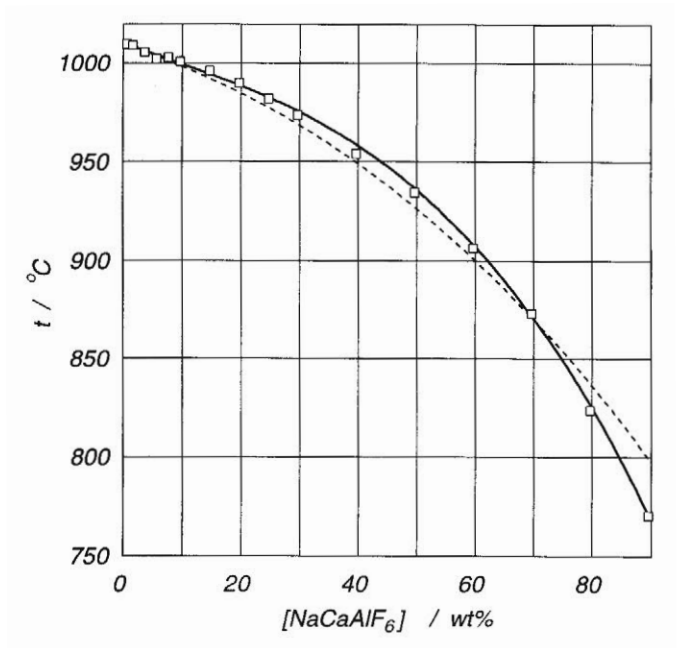


**Figure 5**. Freezing point depression in the system $Na_3AlF_6$-$NaCaAlF_6$. Full line - Eq. (4), broken line - Eq. (4) without crossterms between $CaF_2$ and $AlF_3$.

The maximum is located at about 1.5 wt% excess of $AlF_3$ ($2.89NaF{\cdot}AlF_3$). From the shape of the liquidus curves in the systems NaF-$Na_3AlF_6$ and $Na_3AlF_6$-$AlF_3$, Dewing[25] arrived at the conclusion that cryolite crystallizes as a non-stoichiometric compound from such melts. From electric conductivity measurements and model calculations Dewing[26] found that the maximum was located at the composition $2.846NaF{\cdot}AlF_3$, in fair agreement with the present work. Although there are some uncertainties in the data, it is reasonable to conclude that cryolite melts as a non-stoichiometric compound, and that Dewing's suggestion about premelting and some high temperature solid solution of $AlF_3$ in cryolite is correct.

$Na_3AlF_6$-$CaF_2$. Freezing point depression data from Holm[23] for the binary system $Na_3AlF_6$-$CaF_2$ is replotted and shown in Figure 3. According to Holm, the eutectic point is located at 27.1 wt% $CaF_2$ and 946 °C. With small additions of $CaF_2$, Eqs. (3) and (4) both give $dt/d[CaF_2] = -3.45$ °C/wt%.

$Na_3AlF_6$-LiF. The cryolite liquidus line in the system $Na_3AlF_6$-LiF is shown in Figure 3 as well. The data from Holm[24] are in reasonable agreement with data from the present work. From the cryoscopy equation (3) we obtain $dt/d[LiF] = -10.40$ °C/wt%, whereas Eq. (4) gives -8.90 °C/wt% with small additions.

$Na_3AlF_6$-$Al_2O_3$ and $Na_3AlF_6$-$AlF_3$-$Al_2O_3$. The primary crystallization temperature of cryolite in the binary system $Na_3AlF_6$-$Al_2O_3$ is shown in Figure 4. The two sets of data from Holm and the present work agree well.

It has been proposed[27] that the main species containing oxygen atoms are $Al_2OF_6^{2-}$ and $Al_2O_2F_4^{2-}$. The former dominates at low alumina concentrations, and gives rize to a freezing point depression corresponding to n = 3 new species for each molecule of $Al_2O_3$. This gives $dt/d[Al_2O_3] = -7.93$ °C/wt% according to Eq. (3), which is consistence with Eq. (4). The species $Al_2O_2F_4^{2-}$ gives a freezing point depression corresponding to n = 3/2, and since it dominates at high alumina concentration, the liquidus curve takes a concave shape.

It can be shown that for a given activity of alumina in the melt, the ratio $Al_2OF_6^{2-}/Al_2O_2F_4^{2-}$ will increase with increasing content of $AlF_3$[27]. This implies that the freezing point depression due to $Al_2O_3$ should increase slightly with increasing amounts of $AlF_3$ in the melt. This agrees well with the crossterm between $Al_2O_3$ and $AlF_3$ (denominator, line 4 of Eq. (4)), which was derived from statistic analysis of data in the multicomponent system $Na_3AlF_6$-$AlF_3$-$Al_2O_3$-$CaF_2$-LiF. Crossterms between $Al_2O_3$ and other components were not justified within the experimental uncertainty.

$Na_3AlF_6$-$MgF_2$ and $Na_3AlF_6$-KF. For these systems, the data were fitted to a common single line as shown in Figure 4. The slope of this line (-3.95 °C/wt%) is somewhat smaller than the theoretical freezing point depressions calculated from Equation (3) (-4.33 °C/wt% $MgF_2$ and -4.64 °C/wt% KF).

$Na_3AlF_6$-$AlF_3$-$CaF_2$. The freezing point depression exerted by $CaF_2$ depends on the composition of the system, which can be explained by some combined solid solubility of $CaF_2$ and $AlF_3$ in cryolite. This is demonstrated in Figure 5, showing liquidus data for the system $Na_3AlF_6$-$NaCaAlF_6$. The dashed line, calculated from Eq. (4) omitting the crossterms between $CaF_2$ and $AlF_3$, does not well fit the experimental data.

$Na_3AlF_6$-$AlF_3$-LiF. LiF and $AlF_3$ were added at fixed ratios, corresponding to hypothetical compounds of the type $Li_xAlF_{3+x}$. Some liquidus data are shown in Figure 6. The results indicate a mutual solid solubility effect of LiF and $AlF_3$ in $Na_3AlF_6$.

The results for the system $Na_3AlF_6$-$Li_xAlF_{3+x}$-$CaF_2$ with different values of x are shown in Figure 7, whereas other data obtained in systems with more than three components are given in Table I below. The data did not justify the adding of other cross-terms between different components than those already mentioned.

Comparison with other liquidus equations. A comparison with liquidus equations published by Dewing[9] and by Peterson and Tabereaux[12] is provided in Figure 8. For normal concentrations of $AlF_3$, $CaF_2$, and $Al_2O_3$ (about 10 wt%, 5 wt%, and 3 wt%, respectively) there is reasonable agreement between the three equations. The predicted influence of $CaF_2$ and of $Al_2O_3$ is somewhat different in the three equations, however. The equation presented by Peterson and Tabereaux[12] contains numerous cross-terms between $CaF_2$, $Al_2O_3$ and $AlF_3$, which tends to give erroneous results outside conventional bath compositions. The equation derived by Dewing[9] does not contain any cross terms, which implies that the influence of the variable solid solubility has not been accounted for.

Table I. Experimental liquidus temperatures and liquidus temperatures calculated from Eq. (4) for different melt compositions (wt%) not included in the figures.

| [$AlF_3$] | [$CaF_2$] | [LiF] | [$Al_2O_3$] | Liquidus temp. [°C] Exp. | Eq. (4) |
|---|---|---|---|---|---|
| 5.36 | 4.78 | 4.96 | 4.00 | 929.5 | 929.3 |
| 5.47 | 4.88 | 5.07 | 2.00 | 939.7 | 938.8 |
| 5.76 | 5.17 | 1.78 | 2.00 | 965.1 | 965.2 |
| 5.80 | 5.18 | 1.79 | 4.00 | 953.3 | 954.3 |
| 11.92 | 5.32 | 3.68 | 4.00 | 920.6 | 921.1 |
| 12.17 | 5.42 | 1.88 | 4.00 | 934.6 | 933.4 |
| 12.17 | 5.43 | 3.76 | 2.00 | 931.8 | 930.7 |
| 12.42 | 5.53 | 1.92 | 2.00 | 945.2 | 943.2 |
| 21.00 | 3.50 | 9.00 | 1.00 | 848.0 | 848.8 |
| 21.00 | 3.50 | 9.00 | 2.00 | 840.5 | 841.8 |
| 21.00 | 3.50 | 9.00 | 3.00 | 834.5 | 835.2 |
| 23.00 | 3.50 | 7.10 | 1.00 | 843.7 | 840.4 |
| 23.00 | 3.50 | 7.10 | 2.00 | 835.7 | 833.2 |
| 23.00 | 3.50 | 7.10 | 3.00 | 827.4 | 826.5 |
| 25.00 | 3.50 | 3.50 | 1.00 | 834.5 | 837.2 |
| 25.00 | 3.50 | 3.50 | 2.00 | 826.0 | 830.0 |

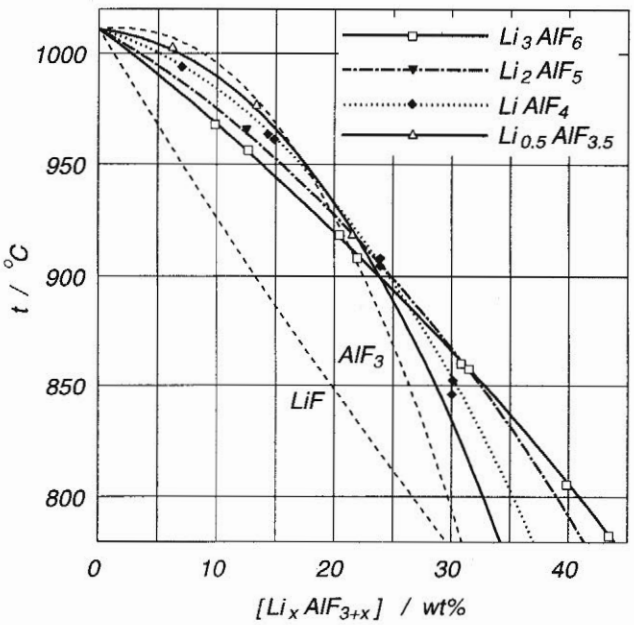


**Figure 6.** Liquidus curves in the system $Na_3AlF_3$-$AlF_3$-LiF. $AlF_3$ and LiF were added at fixed ratios corresponding to hypothetical compounds $Li_xAlF_{3+x}$. The curves represent Eq. (4).

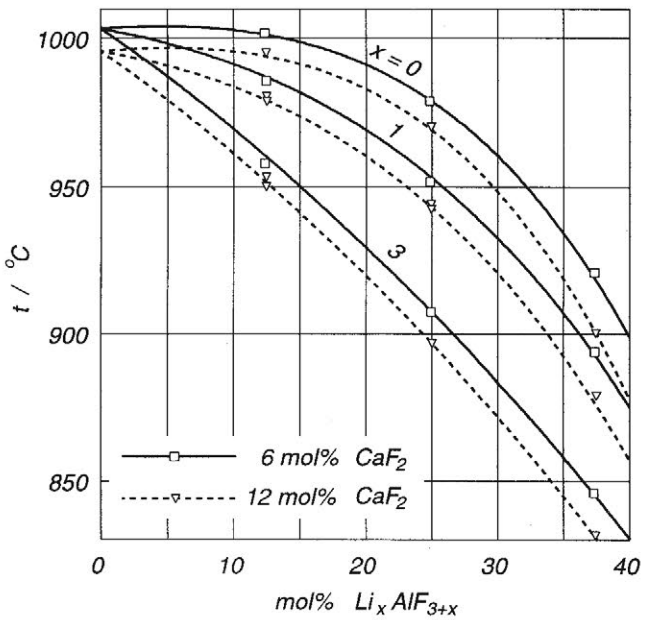


**Figure 7.** Liquidus curves for primary cryolite crystallization in systems of the type $Na_3AlF_6$-$Li_xAlF_{3+x}$-$CaF_2$ with given values for x and $CaF_2$. The curves represent Eq. (4).

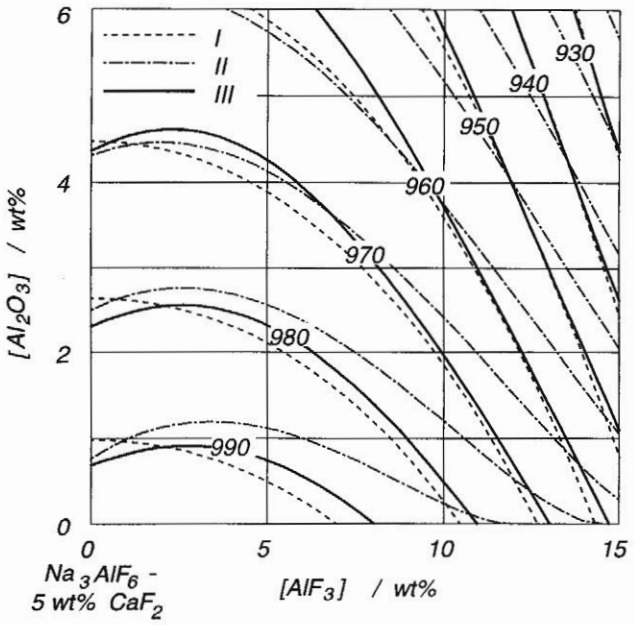


**Figure 8**. Part of the $Na_3AlF_6$ - 5 wt% $CaF_2$ - $AlF_3$ - $Al_2O_3$ phase diagram as calculated from different liquidus equations. I - Dewing[9], II - Peterson and Tabereaux[12], III - This work.

Alumina Solubility

The initial melt compositions (before adding alumina) in the system $Na_3AlF_6$-$AlF_3$-LiF-$CaF_2$-$MgF_2$ were selected as shown in Figure 9. The alumina solubility was usually determined at three different temperatures for each composition. The results presented graphically in Figures 10-18 may be of some interest when selecting low temperature baths for aluminium electrolysis.

The data were fitted to the equation

$$[Al_2O_3]_{sat} = A\left(\frac{t}{1000}\right)^B \quad \text{or} \quad t = 1000\left(\frac{[Al_2O_3]}{A}\right)^{\frac{1}{B}}$$

where

$$A = 11.9 - 0.062[AlF_3] - 0.0031[AlF_3]^2 - 0.50[LiF] - 0.20[CaF_2] - 0.30[MgF_2] + \frac{42\,[LiF]\cdot[AlF_3]}{2000 + [LiF]\cdot[AlF_3]}$$

$$B = 4.8 - 0.048[AlF_3] + \frac{2.2\,[LiF]^{1.5}}{10 + [LiF] + 0.001\,[AlF_3]} \qquad (5)$$

where the square brackets denote wt% of components in the system $Na_3AlF_6$-$Al_2O_3$(sat)-$AlF_3$-$CaF_2$-$MgF_2$-LiF and t is the temperature in °C. The standard deviation between the equation and the experimental points in the temperature range 850 °C-1050 °C was found to be 0.29 wt% $Al_2O_3$ for the 120 points.

The system $Na_3AlF_6$-$AlF_3$. Figure 10 shows the liquidus temperature lines for primary crystallization of both $Na_3AlF_6$ and $Al_2O_3$. It is well established that the $Na_3AlF_6$-$Al_2O_3$ system is a simple eutectic system[17,28]. The alumina saturation concentrations found in the present work are in good agreement with the work of Chin and Hollingshead[14] and Henry and Lafky[29] based on saturation measurements. Other data[15,28] show somewhat higher solubilities, but they may be in agreement when considering the experimental uncertainties.

Data from different sources describing the eutectic point in the $Na_3AlF_6$-$Al_2O_3$ system are given in Table II. At least 50 experimental determinations of the melting point of natural sodium cryolite have revealed that it is 1011±1 °C, when selecting the purest crystals. The melting point of the cryolite used in most of the investigations shown in Table II is lower, which may indicate that some impurities must be present. If this assumption is correct, it may mean that the eutectic temperature should be raised accordingly, bringing most of the data to be consistent with 965±1°C and 10.0±0.3 wt % $Al_2O_3$ as the eutectic point.

Table II. Eutectic temperature ($t_{eut}$) and eutectic alumina concentration ($[Al_2O_3]_{eut}$) in the system $Na_3AlF_6$-$Al_2O_3$ from different sources, compared with the corresponding melting point of the cryolite used ($t_{cry}$).

| Author/ref. | $t_{cry}$ [°C] | $t_{eut}$ [°C] | $[Al_2O_3]_{eut}$ [wt%] |
|---|---|---|---|
| Fenerty and Hollingshead[15] | 1009 | 961 | 10.2 |
| Phillips *et al.*[30] | 1009 | 962 | 10.0 |
| Foster[31] | 1004 | 961 | 10.5 |
| Rolin[32] | 1009 | 960 | 11.5 |
| Brynestad *et al.*[33] | 1011 | 963 | 10.6 |
| Chin *et al.*[14] | 1009 | 962 | 10.0 |
| Holm[34] | 1011 | 963 | 11.2 |
| This work | 1011 | 965.9*) | 10.07*) |

*) From Equations (4) and (5)

The system $Na_3AlF_6$-$AlF_3$-LiF-$Al_2O_3$-$CaF_2$-$MgF_2$. Provided a constant sum [LiF] + [$AlF_3$], the crossterm between $AlF_3$ and LiF in term A of Eq. (5) has its maximum close to the $Li_3AlF_6$ composition. It should be noted, however, that the alumina solubility is more dependent on the temperature in melts with high contents of LiF than in melts high in $AlF_3$ (see Figures 11-14). This indicates that low-melting baths should be based on large additions of $AlF_3$ rather than LiF. This is also evident from Figure 19, which gives corresponding values for the alumina concentration and the temperature along the cryolite/alumina invariant line.

The calculated phase diagram ($Na_3AlF_6$-5 wt% $CaF_2$)-$AlF_3$-$Al_2O_3$ is given in Figure 20.

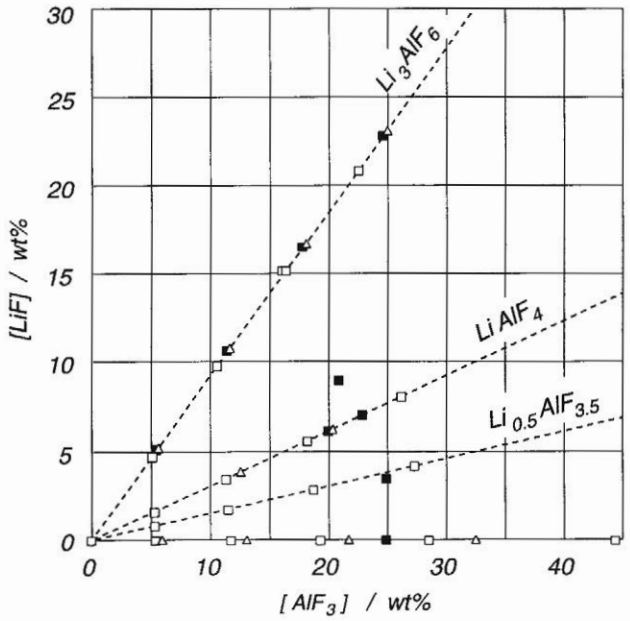


**Figure 9**. Location of experimental points in the system $Na_3AlF_6$-$AlF_3$-LiF-$CaF_2$-$MgF_2$. Open squares - without $CaF_2$ or $MgF_2$, filled squares - addition of up to 6 wt% $CaF_2$, triangles - addition of up to 5.8 wt% $MgF_2$.

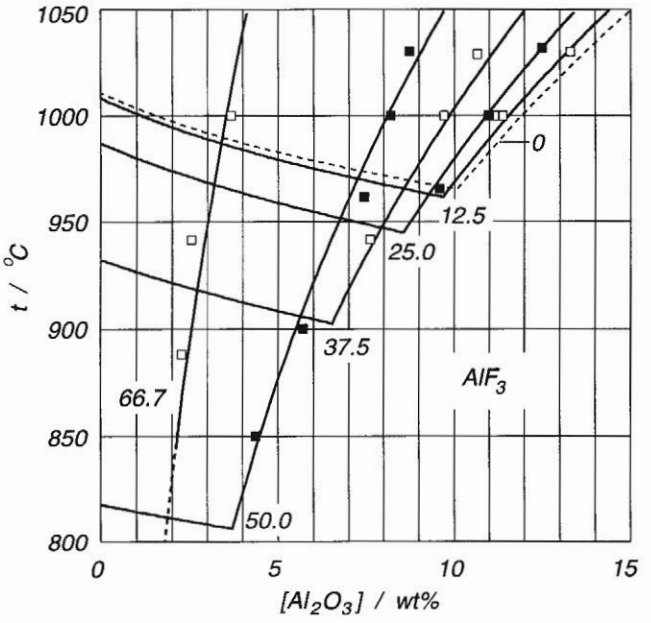


**Figure 11**. The solubility of alumina in the system $Na_3AlF_6$-$AlF_3$-$Al_2O_3$, visualized as quasibinary phase diagrams. The initial (i.e., alumina-free) melt composition (mol% $AlF_3$) is given in the figure. The curves represent Eqs. (4) and (5).

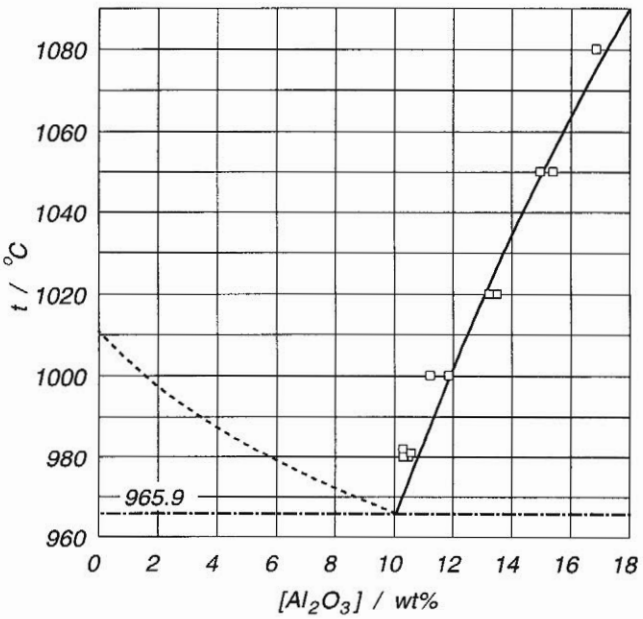


**Figure 10**. The liquidus diagram for the binary system $Na_3AlF_6$ - $Al_2O_3$. Full line - Eq. (5), broken line - Eq. (4).

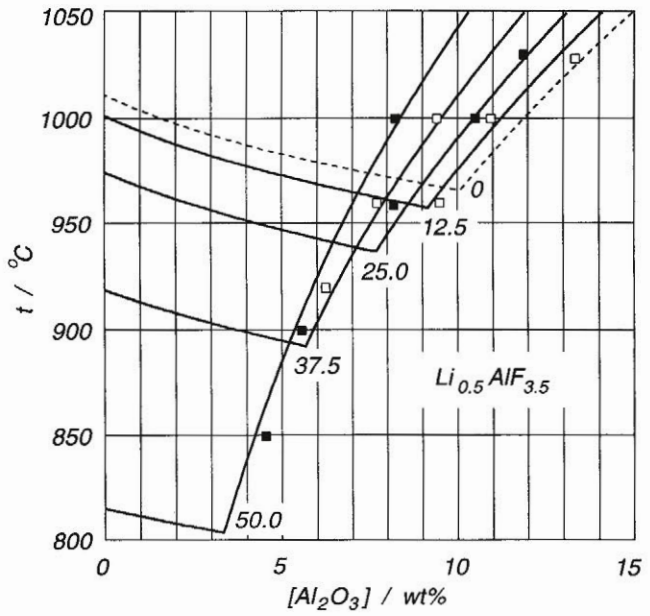


**Figure 12**. The solubility of alumina in the system $Na_3AlF_6$-$Li_{0.5}AlF_{3.5}$-$Al_2O_3$, visualized as quasibinary phase diagrams. The initial (i.e., alumina-free) melt composition (mol% $Li_{0.5}AlF_{3.5}$) is given in the figure. The curves represent Eqs. (4) and (5).

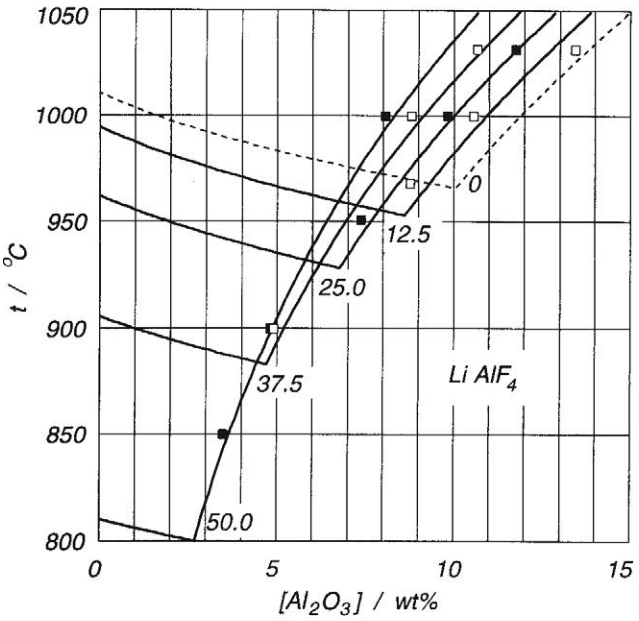


**Figure 13.** The solubility of alumina in the system $Na_3AlF_6$-$LiAlF_4$-$Al_2O_3$, visualized as quasibinary phase diagrams. The initial (i.e., alumina-free) melt composition (mol% $LiAlF_4$) is given in the figure. The curves represent Eqs. (4) and (5).

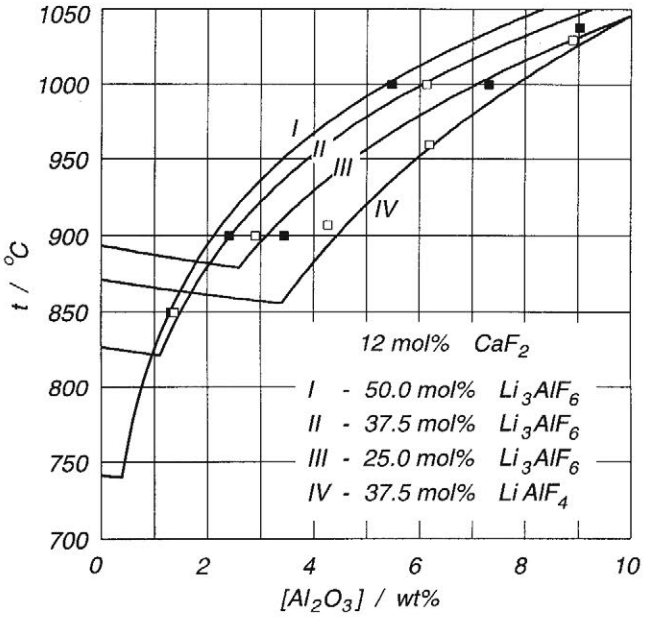


**Figure 15.** The solubility of alumina in the system $Na_3AlF_6$-$AlF_3$-LiF-12 mol% $CaF_2$-$Al_2O_3$, visualized as quasibinary phase diagrams. The initial (i.e., alumina-free) melt composition is given in the figure. The curves represent Eqs. (4) and (5).

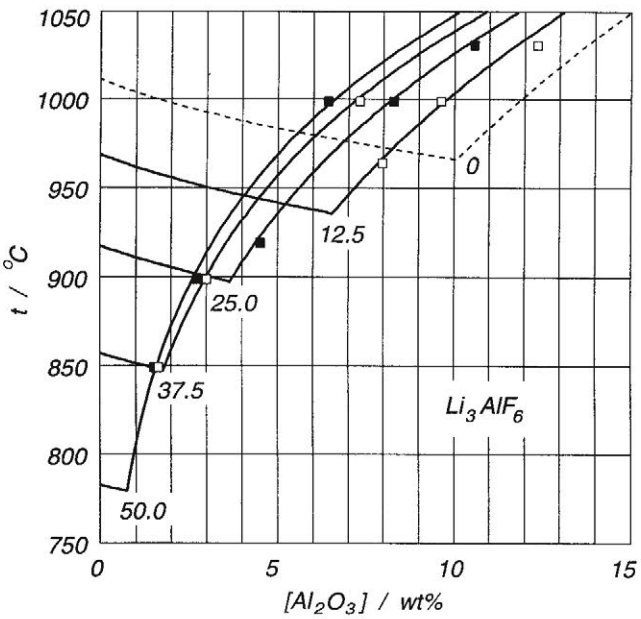


**Figure 14.** The solubility of alumina in the system $Na_3AlF_6$-$Li_3AlF_6$-$Al_2O_3$, visualized as quasibinary phase diagrams. The initial (i.e., alumina-free) melt composition (mol% $Li_3AlF_6$) is given in the figure. The curves represent Eqs. (4) and (5).

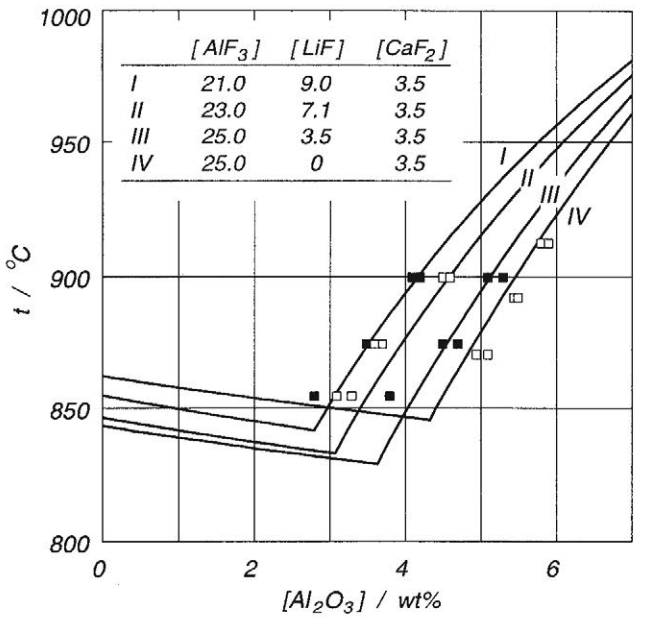


**Figure 16.** The solubility of alumina in the system $Na_3AlF_6$-$AlF_3$-LiF-3.5 wt% $CaF_2$-$Al_2O_3$, visualized as quasibinary phase diagrams. The initial (i.e., alumina-free) melt composition (in wt%) is given in the figure. The curves represent Eqs. (4) and (5).

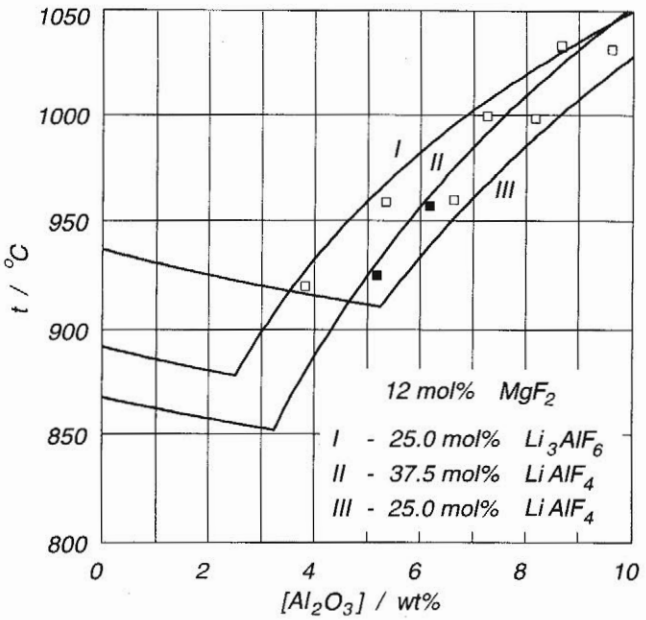


**Figure 17**. The solubility of alumina in the system $Na_3AlF_6$-$AlF_3$-LiF-12 mol% $MgF_2$-$Al_2O_3$, visualized as quasibinary phase diagrams. The initial (i.e., alumina-free) melt composition is given in the figure. The curves represent Eqs. (4) and (5).

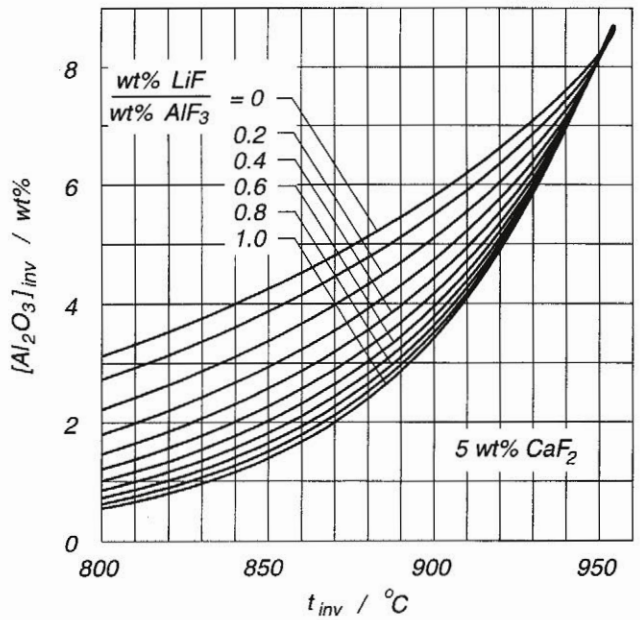


**Figure 19**. Corresponding values for the alumina concentration and the temperature along the $Al_2O_3/Na_3AlF_6$ invariant line in the system $Na_3AlF_6$-5 wt%$CaF_2$-$AlF_3$-LiF at different LiF/$AlF_3$ ratios as given in the figure (calculated from Eqs. (4) and (5)).

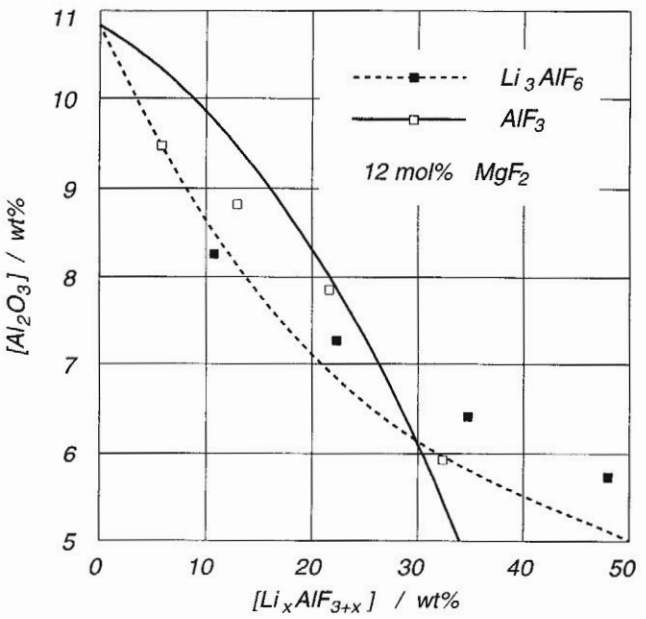


**Figure 18**. The solubility of alumina at 1000 °C in the systems $Na_3AlF_6$-$AlF_3$-$Al_2O_3$-12 mol% $MgF_2$ and $Na_3AlF_6$-$Li_3AlF_6$-$Al_2O_3$-12 mol% $MgF_2$. The curves represent Equation (5).

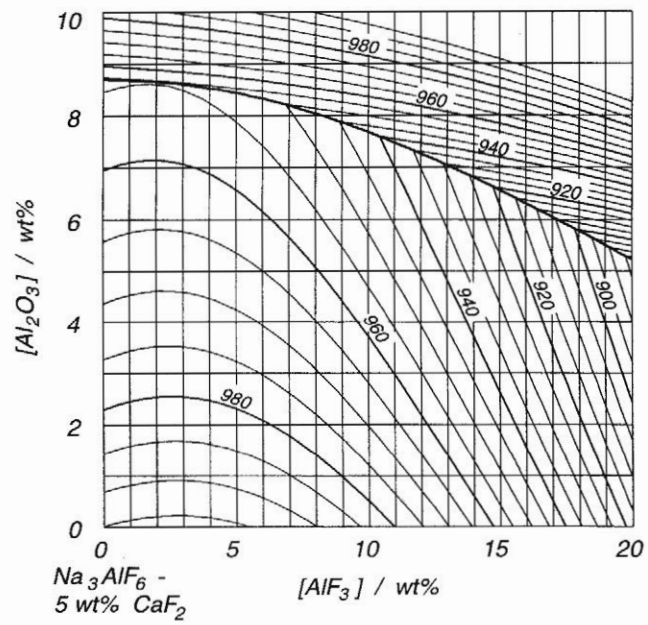


**Figure 20**. Part of the ($Na_3AlF_6$-5 wt% $CaF_2$)-$AlF_3$-$Al_2O_3$ phase diagram, as calculated from Eqs. (4) and (5).

Acknowledgement

Financial support from the Research Council of Norway, from the Norwegian aluminium industry, and from Comalco Research Centre, Victoria, Australia is gratefully acknowledged. Part of the experimental work was carried out by Mr. Reidar Angell Hansen, Mrs. Åse Røstum, and Mr. Odd Skar.

References

1. J.L. Holm: *Trans. Faraday Soc.*, 1962, vol. 58, p. 1104.
2. Å. Sterten and O. Skar: *Aluminium*, 1988, vol. 64, p. 1051.
3. X. Wang, R.D. Peterson and A.T. Tabereaux: Proc. TMS-AIME, Light Metals 1993, p. 247.
4. P. Fellner, S. Midtlyng, Å. Sterten, J. Thonstad: *J. Appl. Electrochem.*, 1993, vol. 23, p.78.
5. R.D. Peterson and X. Wang: Proc. TMS-AIME, Light Metals 1991, p. 331.
6. Å. Sterten, S. Rolseth, E. Skybakmoen, A. Solheim, and J. Thonstad: Proc. TMS-AIME, Light Metals 1988, p. 663.
7. J. Thonstad and A. Solheim: *Aluminium*, 1986, vol. 62, p. 938.
8. T.R. Alcorn, A.T. Tabereaux, N.E. Richards, C.F. Windisch, Jr., D.M. Strachan, J.S. Gregg, and M.S. Frederick: Proc. TMS-AIME, Light Metals 1993, p. 433.
9. E.W. Dewing: *J. Electrochem. Soc.*, 1970, vol. 117, p. 780.
10. S.S. Lee, K. Lei, P. Xu, and J.J. Brown: Proc. TMS-AIME, Light Metals 1984, p. 841.
11. G.L. Bullard and D.O. Przybycien: Proc. TMS-AIME, Light Metals 1986, p. 437.
12. R.D. Peterson and A.T. Tabereaux: Proc. TMS-AIME, Light Metals 1987, p. 383.
13. Å. Røstum, A. Solheim and Å. Sterten: Proc. TMS-AIME, Light Metals 1990, p. 311.
14. D.A. Chin and E.A. Hollingshead: *J. Electrochem. Soc.*, 1966, vol. 113, p. 736
15. A. Fenerty and E.A. Hollingshead: *J. Electrochem. Soc.*, 1960, vol. 107, p. 993.
16. P.A. Foster, Jr.: *J. Amer. Ceram. Soc.*, 1975, vol. 58, p. 288.
17. K. Grjotheim, C. Krohn, M. Malinovsky, K. Matiasovsky and J. Thonstad: Aluminium Electrolysis, 2nd ed., Aluminium-Verlag, Düsseldorf, 1982.
18. J. Thonstad, S. Rønning and P. Entner: Proc. TMS-AIME, Light Metals 1982, p. 485.
19. E. Skybakmoen, A. Solheim, and Å. Sterten: Proc. TMS-AIME, Light Metals 1990, p. 317.
20. H.G. Johansen, Å. Sterten, and J. Thonstad: *Acta Chem. Scand.*, 1989, vol. 43, p.417.
21. E. Skybakmoen, A. Solheim, and Å. Sterten, to be published.
22. Å. Sterten and I. Mæland: *Acta Chem. Scand.*, 1985, vol. 39, p. 241.
23. J.L. Holm: *Acta Chem. Scand.*, 1968, vol. 22, p.1004.
24. J.L. Holm: "Thermodynamic Properties of Molten Cryolite and other Fluoride Mixtures", Thesis, Institute of Inorganic Chemistry, University of Trondheim, NTH, 1971.
25. E.W. Dewing: *Met. Trans.*, 1972, vol. 3, p. 2699.
26. E.W. Dewing: *Met. Trans. B*, 1978, vol. 9B, p. 687.
27. Å. Sterten: *Electrochim. Acta*, 1980, vol. 25, p. 1673.
28. P.A. Foster: *J. Am. Ceram. Soc.*, 1960, vol. 43, p. 66.
29. J.L. Henry and W.M. Lafky: *Ind. Eng. Chem.*, 1956, vol. 48, p. 126.
30. N.W.F. Phillips, R.H. Singleton, and E.A. Hollinghead, *J. Electrochem. Soc.*, 1955, vol. 102, p. 648.
31. P.A. Foster, Jr.: *J. Amer. Ceram. Soc.*, 1970, vol. 53, p. 598.
32. M. Rolin, *Bull. Soc. Chim. France*, 1960, p. 1201.
33. J. Brynestad, K. Grjotheim, F. Grønvold, J.L. Holm, and S. Urnes, *Disc. Faraday Soc.*, 1962, vol. 32, p. 90.
34. J.L. Holm, *Tidsskr. Kjemi, Bergv., Met.*, 1966, vol. 10, p. 165.